Electronic Supplementary Material

Ultrathin nanobelts-assembled Chinese knot-like 3D TiO_2 for fast and stable lithium storage

Qili Wu[1], Shiman He[1], Xianfeng Yang[2], Jingling Yang[1], Gaoren Li[1], Yuying Meng[1], Shengfu Tong[1] (✉), Liqiang Mai[3] (✉), and Mingmei Wu[1] (✉)

[1] *MOE Key Laboratory of Bioinorganic and Synthetic Chemistry, School of Chemistry, Sun Yat-Sen University, Guangzhou 510275, China*
[2] *Analytical and Testing Center, South China University of Technology, Guangzhou 510640, China*
[3] *State Key Laboratory of Advanced Technology for Materials Synthesis and Processing, Wuhan University of Technology, Wuhan 430070, China*

Supporting information to https://doi.org/10.1007/s12274-017-1829-3

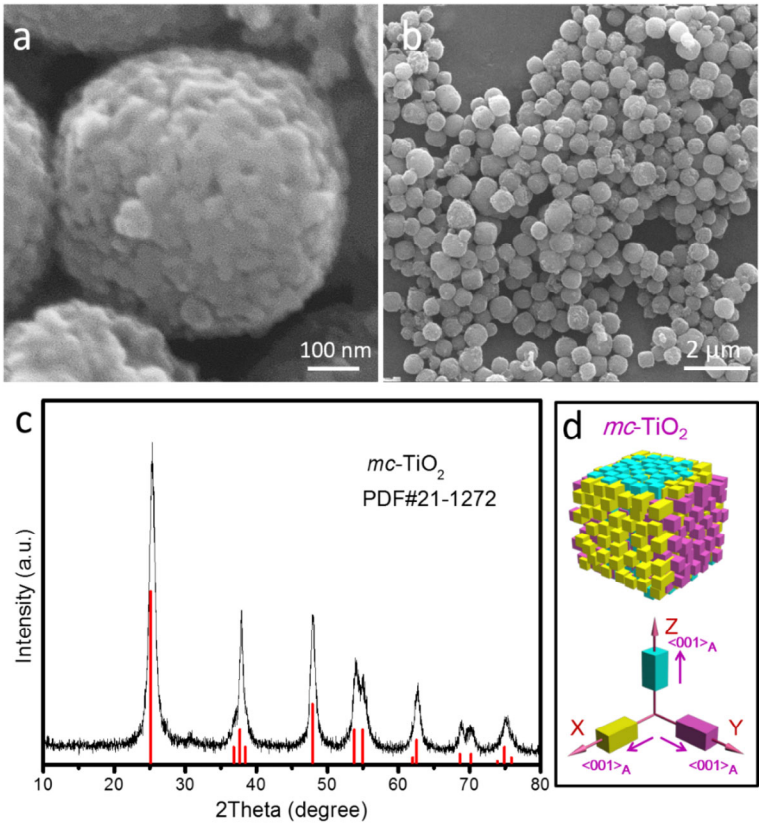

Figure S1 High (a) and low (b) magnification SEM images of the *mc*-TiO_2 microcages, and the corresponding XRD patterns (c). (d) A structure model of *mc*-TiO_2 (up) and the illustration of the perpendicular relationship between the corresponding building blocks (down).

Address correspondence to Mingmei Wu, ceswmm@mail.sysu.edu.cn; Shengfu Tong, tongshf@mail.sysu.edu.cn; Liqiang Mai, mlq518@whut.edu.cn

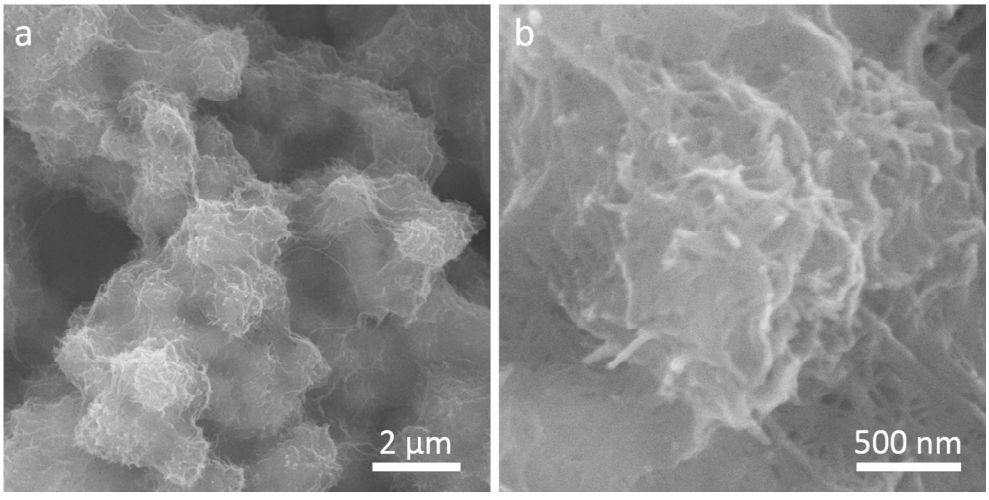

Figure S2 SEM images of 3D NTO.

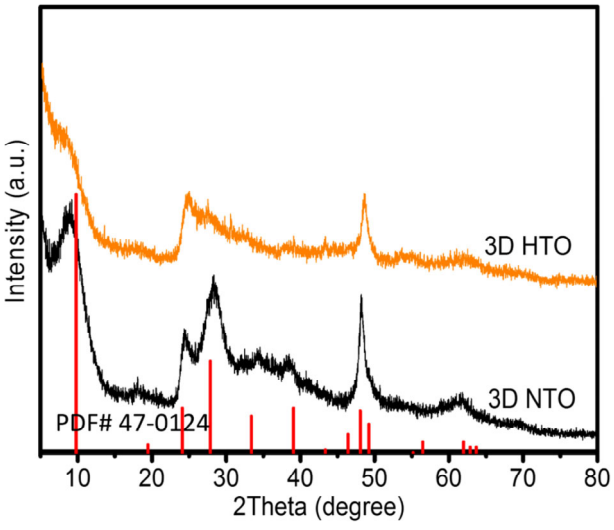

Figure S3 XRD patterns of 3D NTO and 3D HTO. The red lines are the standard diffractions of $H_2Ti_2O_5 \cdot H_2O$ (PDF#47-0124, a = 0.3784 nm, b = 1.803 nm and c = 0.2998 nm).

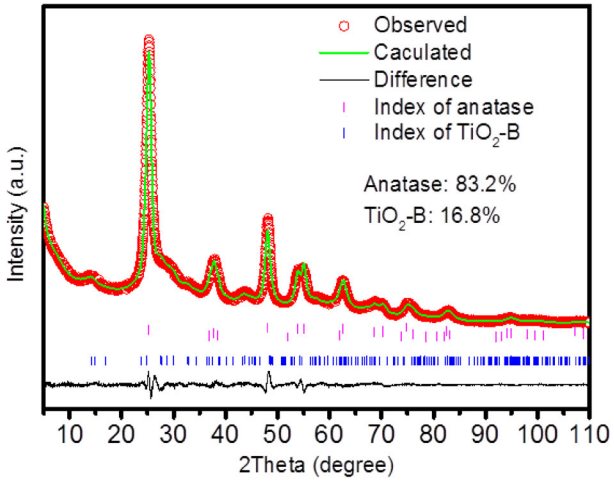

Figure S4 Rietveld refinement analysis of XRD pattern of 3D TiO_2. Anatase: PDF#21-1272, TiO_2-B: PDF#35-0088.

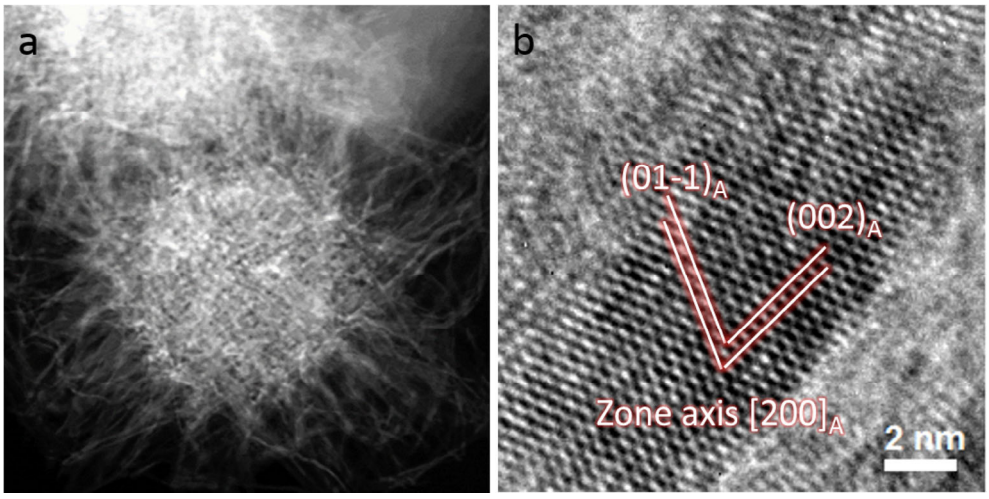

Figure S5 (a) STEM and (b) HRTEM images of 3D TiO_2.

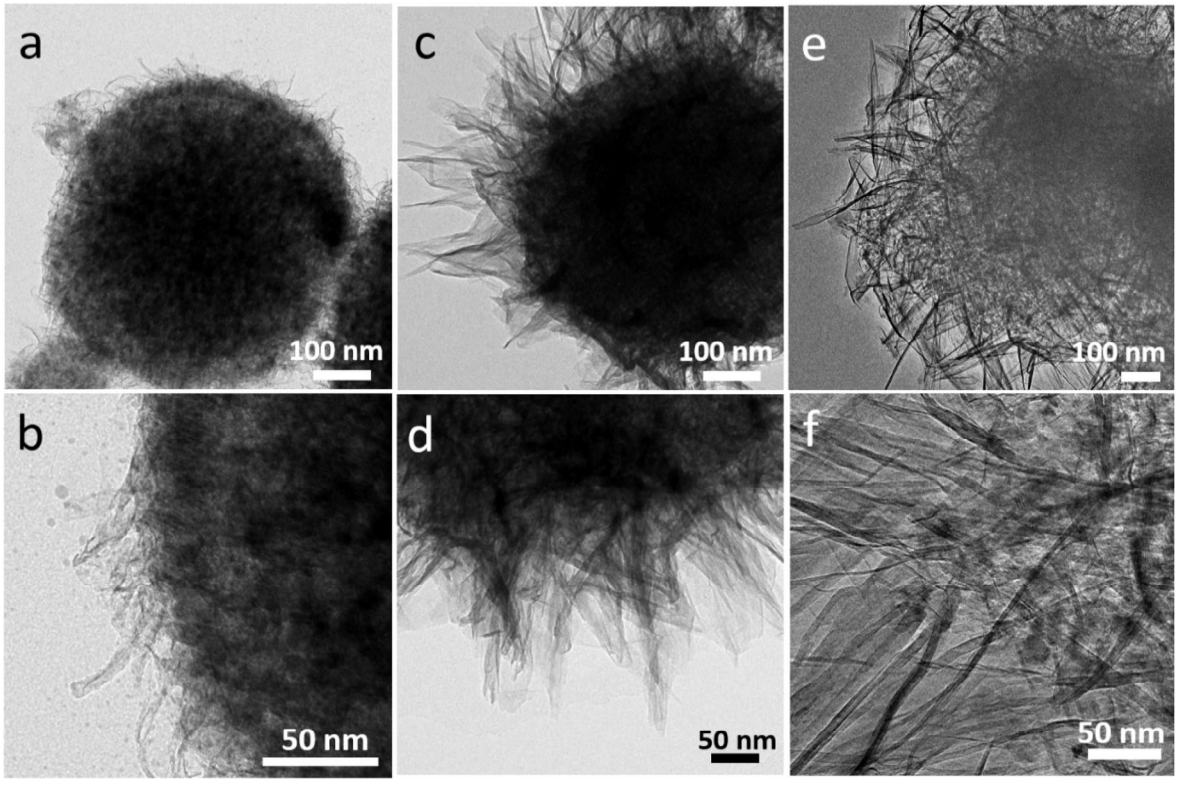

Figure S6 TEM images of *mc*-TiO_2 treated in 10M NaOH for 1 h (a, b), 2 h (c, d), and 4 h (e, f).

When treated with 10 M NaOH for 1 h, some tiny nanosheets were observed at the surface of the microcages (Fig. S6a and S6b). The nanosheets all tilt to the same direction forming a similar angle with the surface of the microcage, confirming that anatase nanoparticles oriented in the same direction will be delaminated in the same direction. These small nanosheets grew to be larger and longer after 2 h reaction (Fig. S6c and S6d). But the interior of the microcage remained non-delaminated. When the reaction time extended to 4 h, 3D nanoarchitecture constructed by perpendicularly oriented ultrathin nanobelts was clearly observed with few anatase nanoparticles inside (Fig. S6e and S6f).

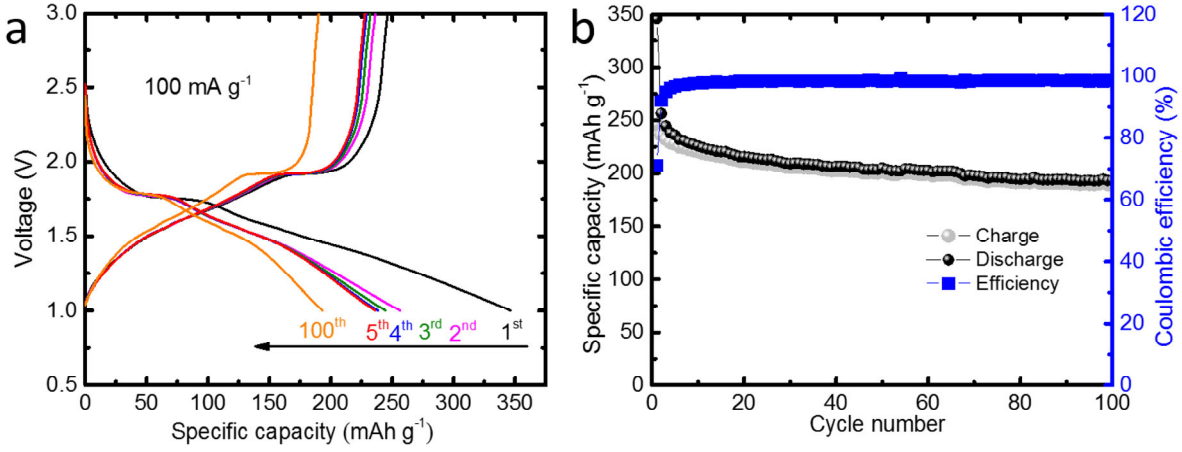

Figure S7 (a) The galvanostatic discharge-recharge curves of 3D TiO_2 at the current densities of 100 mA g^{-1} (0.5 C). (b) Cycling capacity of 3D TiO_2 at 100 mA g^{-1} (0.5 C) for 100 cycles.

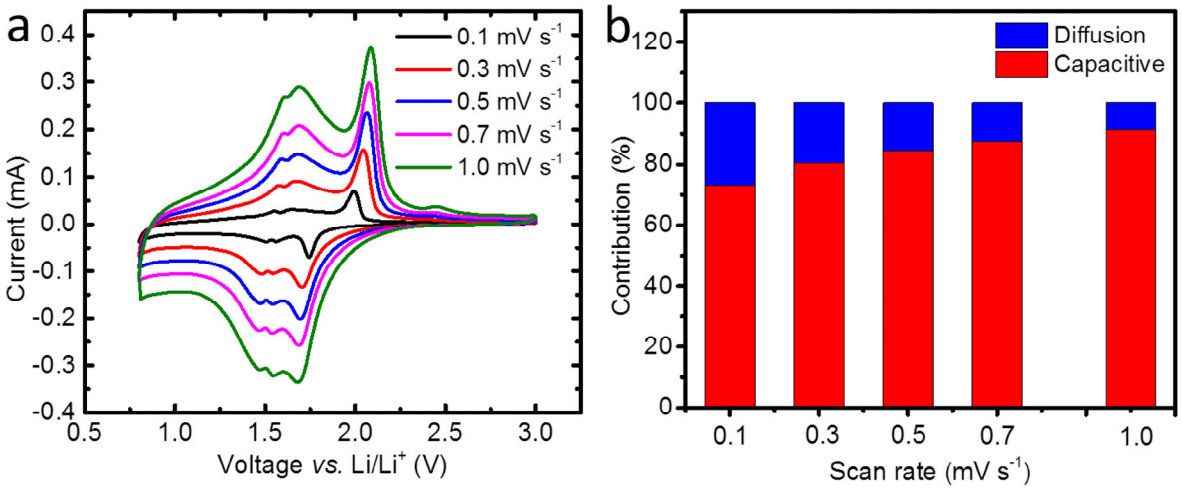

Figure S8 (a) CV curves of 3D TiO_2 at the scan rates from 0.1 to 1 mV s^{-1}. (b) Normalized contribution ratio of capacitive effect (red) and diffusion-controlled reactions (blue) at the corresponding scan rates in (a).

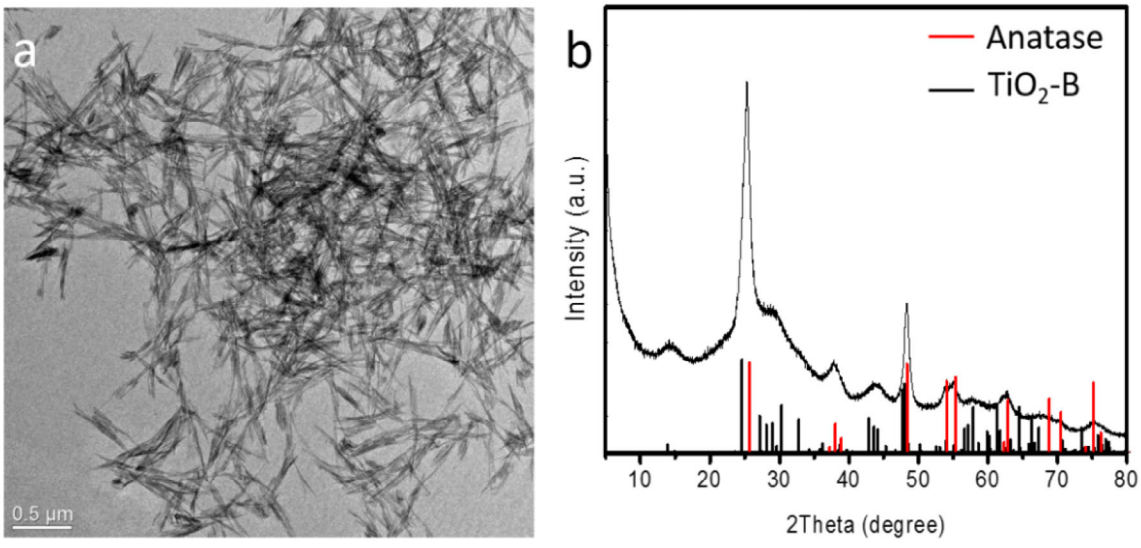

Figure S9 TEM image (a) and XRD patterns (b) of dispersive TiO_2 nanobelts.

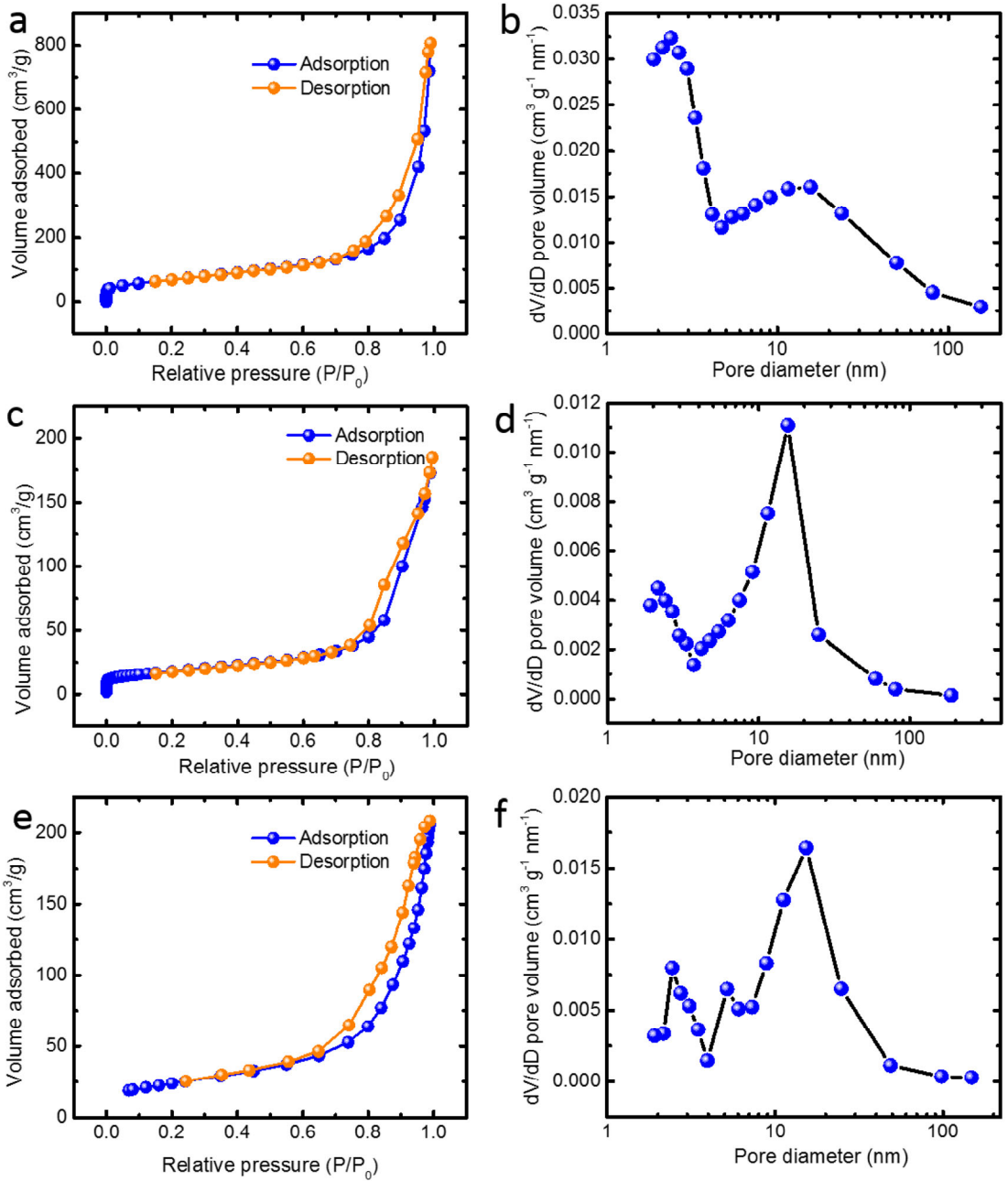

Figure S10 Nitrogen adsorption and desorption isotherms and the pore size distributions of dispersive nanobelts (a, b), AB550 (c, d) and *mc*-TiO_2-400 (e, f).

Table S1 Porous structure parameters of 3D TiO_2, dispersive nanobelts, AB550, and *mc*-TiO_2-400.

Samples	BET surface area (m^2 g^{-1})	Pore volume (cm^3 g^{-1})	Average pore size (nm)
3D TiO_2	302	1.23	11
Dispersive nanobelts	247	1.25	2.5 and 14
AB550	62.3	0.29	15
mc-TiO_2-400	79.1	0.42	2.5 and 15

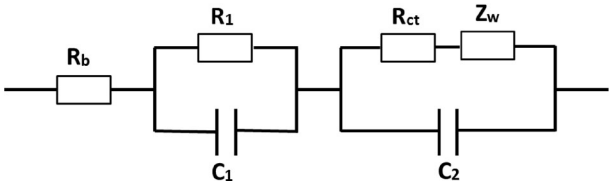

Figure S11 A proposed equivalent circuit for the data in Fig. 3d.

Table S2 Fitted Impedance Parameters of the Equivalent Circuit in Fig. S10.

Sample	R_b/Ohm	R_1/Ohm	R_{ct}/Ohm	Z_W/Ohm
3D TiO_2	1.74	12.2	61.8	120
Dispersive TiO_2	2.05	16.7	114	258
AB550	1.60	17.5	102	157
mc-TiO_2-400	2.07	29.9	132	304

The lithium-ion diffusion coefficients of the four samples are estimated using the inclined lines in the Warburg region and based on the following equation (Eq. s1):

$$D_{Li} = \frac{R^2T^2}{2A^2n^4F^4C^2\sigma^2} \quad \text{(S1)}$$

where R is the gas constant (R = 8.314 J mol^{-1} K^{-1}), T is the absolute temperature (T = 298 K), A is the surface area of the cathode (A = 1.13 cm^2), n is the number of electrons per molecule during reaction (n = 1), F is the Faraday constant (F = 96485 C/mol), C is the concentration of lithium ions (C = 7.69×10^{-3} mol cm^{-3}), and σ is the Warburg factor which can be determined by linearly fitting the Z' *vs.* the square root of frequency $\omega^{-1/2}$. The lithium ion diffusion coefficients in the 3D TiO_2, dispersive nanobelts, AB550 and *mc*-TiO_2-400 were calculated to be 8.37×10^{-15}, 3.29×10^{-15}, 5.44×10^{-14}, 6.91×10^{-14} cm^2 s^{-1}. These results conflict with the lithium storage performances presented in Figure 3c, therefore, the superior lithium storage performance of 3D TiO_2 can be attributed to the high surface area and in favored pseudocapacitance at high current rates.

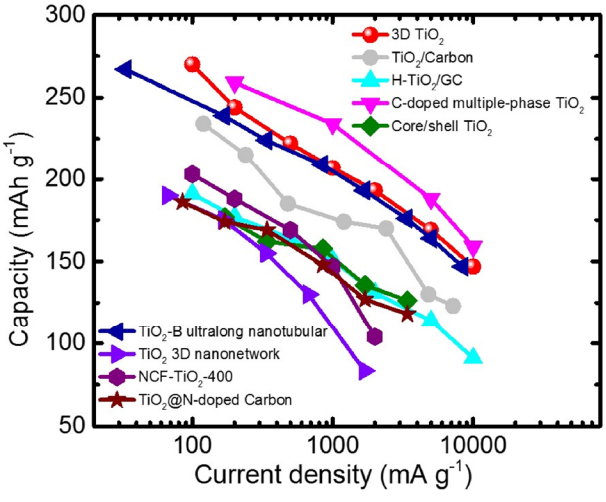

Figure S12 Rate performance comparison of the as-prepared 3D TiO_2 and other recently reported TiO_2 nanostructures. 3D TiO_2 (this work, 70:20:10), TiO_2/Carbon (80:15:5) [1], H-TiO_2/GC (90:0:10) [2], C-doped multiple-phase TiO_2 (80:15:5) [3], core/shell TiO_2 (70:20:10) [4], TiO_2-B ultralong nanotubular (100:0:0) [5], 3D TiO_2 nanonetwork (66:26:8) [6], NCF-TiO_2-400 (100:0:0)[7] and TiO_2@N-doped Carbon (50:30:20) [8].

Table S3 Cycling stability comparison of 3D TiO_2 and other reported TiO_2 nanostructures.

Sample	Current density (mA g^{-1})	Initial/Final capacity (mAh g^{-1})	Cycle number	Capacity retention	Capacity fading of each cycle (mAh g^{-1})
3D TiO_2 (this work)	10000	167/130	3000	77.8%	0.0123
TiO_2/Carbon [1]	1200	174/154	300	88.5%	0.0667
H-TiO_2/GC [2]	1000	150/137	1000	91.3%	0.012
C-doped multiple-phase TiO_2 [3]	2000	220/204	280	92.7%	0.571
Core/shell TiO_2 [4]	170	385/151	100	39.2%	2.34
TiO_2-B ultralong nanotubular [5]	8400	175/114	10000	65.1%	0.0061
3D TiO_2 nanonetwork [6]	335	154/128	200	83.1%	0.13
NCF-TiO_2-400 [7]	1000	149/223	100	66.8%	0.74
TiO_2@N-doped Carbon [8]	1700	130/117	2000	90%	0.0065

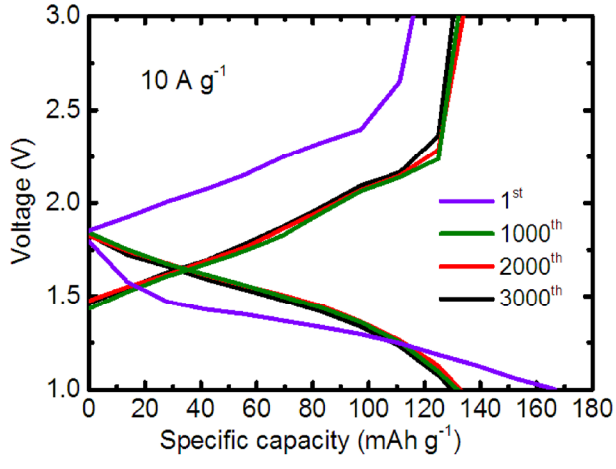

Figure S13 The galvanostatic discharge-recharge curves of 3D TiO_2 at the current density of 10 A g^{-1} (50 C).

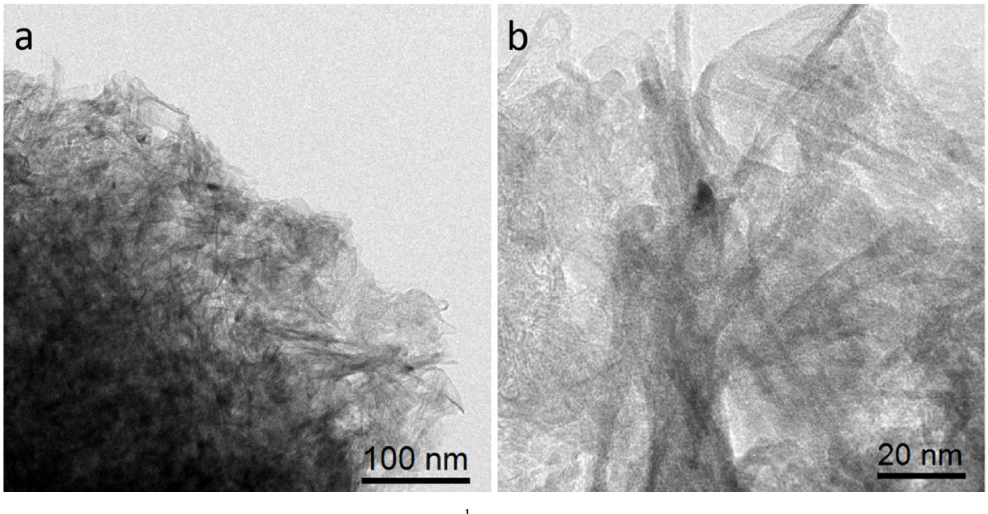

Figure S14 TEM images of 3D TiO_2 after 1000 cycles at 1 A g^{-1} (5 C).

References

[S1] Cheng, Y. H.; Chen, Z.; Wu, H. B.; Zhu, M. F.; Lu, Y. F. Ionic Liquid-Assisted Synthesis of TiO_2-Carbon Hybrid Nanostructures for Lithium-Ion Batteries. *Adv. Funct. Mater.* **2016**, *26*, 1338-1346.

[S2] Liu, H.; Li, W.; Shen, D.; Zhao, D.; Wang, G. Graphitic Carbon Conformal Coating of Mesoporous TiO_2 Hollow Spheres for High-Performance Lithium Ion Battery Anodes. *J. Am. Chem. Soc.* **2015**, *137*, 13161-13166.

[S3] Li, Y.; Shen, J.; Li, J.; Liu, S.; Yu, D.; Xu, R.; Fu, W.-F.; Lv, X.-J. Constructing a novel strategy for carbon-doped TiO_2 multiple-phase nanocomposites toward superior electrochemical performance for lithium ion batteries and the hydrogen evolution reaction. *J. Mater. Chem. A* **2017**, *5*, 7055-7063.

[S4] Cai, Y.; Wang, H. E.; Zhao, X.; Huang, F.; Wang, C.; Deng, Z.; Li, Y.; Cao, G. Z.; Su, B. L. Walnut-like Porous Core/Shell TiO_2 with Hybridized Phases Enabling Fast and Stable Lithium Storage. *ACS Appl. Mater. Interfaces* **2017**, *9*, 10652-10663.

[S5] Tang, Y.; Zhang, Y.; Deng, J.; Wei, J.; Tam, H. L.; Chandran, B. K.; Dong, Z.; Chen, Z.; Chen, X. Mechanical Force-Driven Growth of Elongated Bending TiO_2-based Nanotubular Materials for Ultrafast Rechargeable Lithium Ion Batteries. *Adv. Mater.* **2014**, *26*, 6111-6118.

[S6] Kim, S.-W.; Han, T. H.; Kim, J.; Gwon, H.; Moon, H.-S.; Kang, S.-W.; Kim, S. O.; Kang, K. Fabrication and Electrochemical Characterization of TiO_2 Three-Dimensional Nanonetwork Based on Peptide Assembly. *ACS Nano* **2009**, *3*, 1085-1090.

[S7] Chu, S.; Zhong, Y.; Cai, R.;Zhang, Z.; Wei, S.; Shao, Z. Mesoporous and Nanostructured TiO_2 layer with Ultra-High Loading on Nitrogen-Doped Carbon Foams as Flexible and Free-Standing Electrodes for Lithium-Ion Batteries. *Small* **2016**, *12*, 6724-6734.

[S8] Zhu, H.; Jing, Y.;Pal, M.; Liu, Y.;Liu, Y.;Wang, J.;Zhang, F.; Zhao, D. Mesoporous TiO_2@N-doped carbon composite nanospheres synthesized by the direct carbonization of surfactants after sol-gel process for superior lithium storage. *Nanoscale* **2017**, *9*, 1539-1546.